The following article appeared in *Journal of Applied Physics 120, 123106 (2016);* and may be found at https://doi.org/10.1063/1.4963365

Platinum nanoclusters in silica: Photoluminescent properties and their application for enhancing the emission of silicon nanocrystals in an integrated configuration

J. Bornacelli, H. G. Silva-Pereyra, L. Rodríguez-Fernández, M. Avalos-Borja, and A. Oliver

Citation: Journal of Applied Physics **120**, 123106 (2016); doi: 10.1063/1.4963365
View online: https://doi.org/10.1063/1.4963365
View Table of Contents: http://aip.scitation.org/toc/jap/120/12
Published by the American Institute of Physics

JOURNAL OF APPLIED PHYSICS **120**, 123106 (2016)

Platinum nanoclusters in silica: Photoluminescent properties and their application for enhancing the emission of silicon nanocrystals in an integrated configuration

J. Bornacelli,[1,a)] H. G. Silva-Pereyra,[2] L. Rodríguez-Fernández,[1] M. Avalos-Borja,[2,3] and A. Oliver[1]
[1]*Instituto de Física, Universidad Nacional Autónoma de México, 04510 México, DF, Mexico*
[2]*IPICyT, Division de Materiales Avanzados, Camino a la presa San Jose 2055, San Luis Potosi, SLP 78216, Mexico*
[3]*Centro de Nanociencias y Nanotecnologia – Universidad Nacional Autónoma de México, A. Postal 2681, Ensenada, BC, Mexico*

(Received 1 June 2016; accepted 13 September 2016; published online 26 September 2016)

We studied photoluminescence of ion implanted platinum nanoclusters embedded in silica. Pt ions were implanted at 2 MeV and the Pt nanoclusters were then nucleated by thermal treatment under either argon, air, or a reducing atmosphere of hydrogen and nitrogen. The nanoclusters showed broad photoluminescence spectra (400 to 600 nm) with a maximum intensity at 530 nm. The photoluminescence intensity of the Pt nanoclusters was sensitive to the ion fluence used during the ion implantation, and luminescence quenching was observed in samples fabricated at high Pt-ion fluence. A hybrid system composed of silicon nanocrystals and platinum nanoclusters embedded in a silica matrix was also made. The photoluminescence of the hybrid system spanned the entire visible spectrum, and emission from the silicon nanocrystals was enhanced. *Published by AIP Publishing.* [http://dx.doi.org/10.1063/1.4963365]

I. INTRODUCTION

Noble metal nanoparticles have attracted considerable research interest over the last few decades in physics, chemistry, and material science owing to their unique plasmonic properties.[1–6] When metal nanoparticles are reduced in size (<2 nm), new and interesting properties emerge, such as fluorescence[7,8] and magnetism.[9] Such nanoparticles are often referred to as nanoclusters because of their very small size (∼1 nm). Metal nanoclusters are too small to possess a continuum of density of states, which is necessary to support the plasmon characteristics of large free electron metal nanoparticles.[10] In the nanocluster size regime, strong confinement of electrons results in discrete, quantum-confined electronic transitions, leading to molecular-like properties and strong photoluminescence (PL).[11,12] Metal clusters made of Au and Ag have been widely studied, and several synthesis methods have been used to modify and enhance their fluorescence emission properties.[7,8,11–16] The synthesis of metal nanoclusters of Au, or Ag, embedded in solid matrices has also been studied because of a wide variety of potential applications in nonlinear optics, nanophotonics, and optical communication technologies.[17–19] Although much research has focused on the catalytic activity of nanoparticles made of Pt (another noble metal), the optical properties of these materials have been less well studied. Recently, some authors have reported the fluorescence properties of colloidal Pt nanoclusters (Pt-ncs) synthesized by chemical methods.[20–25] The nanoclusters showed green photoluminescence emission centered around 500 nm with a quantum yield of about 17%. Nano-island films of Pt nanoparticles have also shown micro-photoluminescence emission in the visible light region.[26] Platinum nanoparticles embedded in a silica matrix have been previously synthesized.[27–29] We recently studied the PL emission characteristics of Pt-ncs embedded in SiO_2 and observed quenching of emission for nanoparticles larger than 2 nm in diameter, as plasmonic properties started to emerge.[30] Nanoclusters embedded in glasses are chemically and mechanically stable systems of emissive nanoclusters. These materials are important for technological applications in photonics and optoelectronics as solid state light sources or nano-antenna to transfer electromagnetic energy to another emitting species.[19,31] In this work, we report the synthesis of ion implanted Pt-ncs embedded in silica, synthesized with exposure to three different annealing atmospheres (neutral, oxidizing, or reducing). We investigated the optical properties of the Pt-ncs, including absorption and photoluminescence spectroscopies. We also studied variations in the optical properties of samples with higher Pt-ncs concentrations, which we synthesized using higher ion implantation fluencies. Finally, we synthesized a hybrid system composed of two emitting species, silicon nanocrystals (Si-NCs) and Pt-ncs, both embedded in a silica matrix. This hybrid system emitted light with a broadband spectrum covering the entire visible spectrum, making the sample a bright white PL emitter. We discuss the optical interaction between these two emitter types based on our experimental results.

II. EXPERIMENTAL

Pt-ncs were synthesized by metal ion implantation in a high purity silica matrix (suprasil 300). We implanted the Pt ions at room temperature using an accelerating voltage of 2 MeV at the 3 MV Tandem accelerator (NEC 9SDH-2

[a)] E-mail: jhbornacelli@gmail.com

Pelletron) facility at the *Instituto de Física of the Universidad Nacional Autónoma de México* (IFUNAM). The fluencies used were 1.1×10^{16} (sample A), 2.5×10^{16} (sample B), and 7×10^{16} (sample C) Pt-ions/cm^2. Sample B was cut into three smaller pieces, each of which was heated at 600 °C under argon [Sample B(Ar)], air [Sample B(Air)], or a reducing atmosphere (RA) of 50% N_2 and 50% H_2 [Sample B(RA)]. Samples A and C were also thermally annealed at 600 °C under a reducing atmosphere (Samples A(RA) and C(RA)). We calculated the concentration profile of implanted Pt using SRIM code[32,33] and confirmed these calculations experimentally using Rutherford backscattering spectrometry (RBS),[34] with a 2 MeV $^4He^{++}$ beam.

A second set of samples was synthesized to create a hybrid system of Si-NCs and Pt-ncs, embedded in the same silica matrix. We first implanted a piece of silica with Si ions at 1.5 MeV and a fluence of approximately 2.5×10^{17} ions/cm^2. The sample was then heated under a RA at 1100 °C for 1 h to nucleate the Si-NCs inside the silica matrix. The sample was cut into three smaller pieces, two of which were implanted with 1.9-MeV Pt ions at a fluence of 4.9×10^{16} ions/cm^2. The sample without Pt ions was used as a reference (Si-NCs). At 1.9 MeV, the Pt ion distribution does not spatially overlap with the previously formed Si-NCs, which minimized damage to the nanocrystals. Finally, one of the pieces implanted with Pt ions was heated at 600 °C under RA for 1 h to form Pt-ncs (sample Si-NCs+Pt-ncs). The third sample with Si-NCs and Pt ions, but not subjected to a thermal treatment, was used as a reference sample (Si-NCs+Pt).

PL measurements were performed at room temperature with excitation at 250 and 355 nm using ps pulses at 10 Hz from a combined laser system PL2143A + PG401/SH manufactured by EKSPLA. We measured the PL signal with a 1000 micron optical fiber and Ocean Optics USB2000+ spectrometer. PL spectra were measured with excitation at 250 nm to allow detection of photoluminescence from defects produced in the silica matrix after ion implantation.[35–37] We measured the photoluminescence versus excitation pump pulse fluence at 355 nm for the samples with Pt-ncs (samples A(RA) and C(RA)). We monitored the maxima of the PL spectra every 1 s over 1 min, for each excitation pump pulse fluence. All measurements were performed while maintaining a constant illumination area (~7.2 mm^2) over the sample constant using a mechanical aperture. The optical absorption of all the samples was measured with a Varian Cary 5000 UV-VIS spectrophotometer. The Pt-ncs were observed by an FEI Tecnai F30 transmission electron microscope (FEG-TEM 300 kV) in the scanning transmission electron microscope mode (STEM) with a HAADF detector (Z-contrast).

III. RESULTS AND DISCUSSION

Figure 1 shows the PL spectra of samples implanted with Pt ions and annealed under three different atmospheres: a reducing atmosphere [B(RA)], argon [B(Ar)], and air [B(Air)]. Figures 1(a) and 1(b) show PL spectra observed by excitation at 250 and 355 nm, respectively. The PL spectra of an as-implanted sample are also shown, i.e., a sample not subjected to a thermal treatment. All the annealed samples featured similar PL spectra in the range of 400–700 nm, with a peak at 530 nm. In Figure 2, we show an STEM micrograph of a sample synthesized under the same conditions and annealed under a RA at 600 °C. The energy-dispersive X-ray spectroscopy (EDS) data shown in Figure 2(b) confirmed the presence of nanoclusters composed of platinum. Figure 2(c) shows the size distribution of the Pt-ncs observed in the micrograph of Figure 2(a), as having diameters around 1.0 ± 0.5 nm. Therefore, the emission observed from excitation at 355 nm likely comes from the Pt-ncs formed inside the silica matrix.

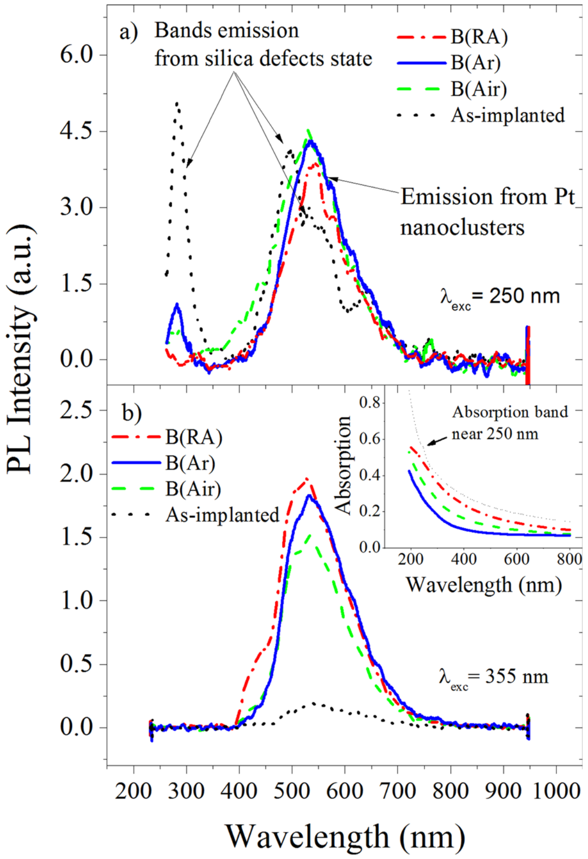

FIG. 1. Photoluminescence spectrum of silica implanted with Pt ions at 2 MeV and annealed under different atmospheres: reducing atmosphere, B(RA) (Dashed-dotted red curve); air, B(Air) (Dashed green curve); and argon, B(Ar) (Continuous blue curve). A spectrum of the unannealed Pt-ion implanted silica (as-implanted sample) is shown for comparison (Dotted black curve). Excitation was at 250 nm (Figure 1(a)) and 355 nm (Figure 1(b)). The inset in Figure 1(b) shows the optical absorption spectra of the samples.

The spectra of the as-implanted sample showed differences when excited at 250 and 355 nm. These can be attributed to luminescence from silica defect states in the sample that were induced by irradiation with Pt ions. The emission bands from the as-implanted sample are related to defect states produced in the silica matrix. We used peak fitting (not shown here) to identify five emission bands at 289, 450, 489, 550, and 650 nm. The ultraviolet (289 nm) and blue (450 and 489 nm) emission bands are produced by B_2 defects.[36–39] The green emission band at 550 nm can be assigned to peroxide radical oxygen.[40–43] The red emission band at 650 nm is produced by non-bridged oxygen hole centers.[37]

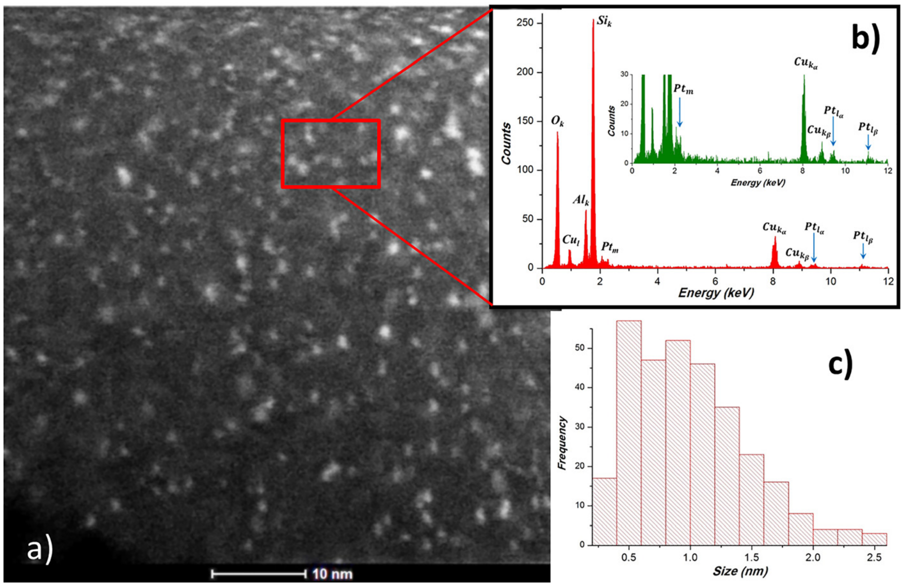

FIG. 2. (a) STEM image of a sample containing Pt nanoclusters. The sample was synthesized in a similar way to sample B(RA). (b) EDS spectra confirmed that the clusters contain platinum. The Pt peaks in the EDS spectra had lower intensity than those of the silica matrix (SiO_2) because of the relatively small amount of implanted Pt ions. (c) Histogram of the particle size distribution of the image in (a).

The inset of Figure 1(b) shows the absorption spectra of the samples. The as-implanted sample showed the characteristic absorption band related to defect states in the silica matrix (B_2 defects); however, the annealed sample did not exhibit this absorption band because the thermal treatment passivated these defect states. However, some weak PL emission remained at 289 nm due to the presence of B_2 defects, as shown in Figure 1(a). This emission band was absent in the sample annealed under a RA. This may be explained by the effective passivation of defects in the silica matrix when the sample was thermally annealed under the reducing atmosphere. We observed no defect state emission using excitation at 355 nm, which is above the defect state absorption at 250 nm. We deduced that the observed PL spectra of the as-implanted sample with excitation at 355 nm (Figure 1(b)) are related to the Pt-ncs formed inside the silica. The PL spectrum of this sample was similar to those of the annealed samples but with a lower intensity.

The sample annealed under air featured a broad intense PL spectrum when excited at 250 nm. However, under excitation at 355 nm, this sample showed a narrower emission spectrum of lower intensity (Figure 1(b)). This may be explained by residual defects in the silica matrix of the samples annealed under argon and air at 600 °C. Silica defects can be photostimulated when excited at 250 nm but not at 355 nm.[30] This means that the PL spectra of the B(Ar) and B(Air) samples in Figure 1(a) have small contributions to their PL emission from silica defects. The small differences in the PL spectra of the annealed samples under excitation at 355 nm can be understood in terms of the annealing atmosphere. It has been determined that thermal annealing under a RA or air results in formation of larger Pt nanoparticles, because of a higher nucleation rate.[29] PL intensity depends strongly on the size of the Pt nanoparticles, with smaller Pt nanoparticles exhibiting higher PL intensities.[30] Thus, samples annealed under air likely featured larger Pt-nanoclusters, which may explain their lower PL intensities.

The PL emission properties of metal nanoclusters depend strongly on their size. In general, below 2 nm, metal nanoclusters exhibit efficient PL emission because of discretization of their electronic levels. Optical transitions in metal nanoclusters can only take place between an occupied ground state and unoccupied excited state above the Fermi level. The mechanism of PL in Ag or Au nanoclusters is mainly attributed to interband transitions between sp to d-like levels or from transitions between the HOMO and LUMO gap formed in the sp-levels of the nanoclusters induced by energy level discretization.[12,15,44] It has been determined that smaller Au nanoclusters emit light at shorter wavelengths.[8,10] Considering that the implanted Pt-ncs feature a certain size distribution, as shown by the STEM image in Figure 2, this may contribute to broadening of the PL spectra. Although the exact mechanism of PL emission from Pt-ncs remains unclear, it is known that their electronic configuration is characterized by discrete electronic levels, resulting in optical transition such as absorption and emission of light. Moreover, Pt-ncs can adsorb hydrogen to their surface and introduce d-electron vacancies above the Fermi level of the Pt nanoparticles, which affects their absorption and emission properties.[29,30,45,46] This might explain why the PL intensity of the sample annealed under a reducing atmosphere was slightly higher than that of the sample annealed under argon, as shown in Figure 1(b).

To gain greater insight into the PL of the Pt-ncs, we synthesized three samples using different ion fluencies during implantation. Figure 3 shows the PL intensity of three samples implanted with Pt ions at (A) $1.1 \times 10^{16}/cm^2$, (B) $2.5 \times 10^{16}/cm^2$, and (C) $7.0 \times 10^{16}/cm^2$, and then thermally annealed under RA at 600 °C. The inset of Figure 3 shows the depth profile concentration of each sample as measured by RBS. The sample with the highest PL intensity was formed at the lowest ion fluence.

Figure 4 shows the corresponding optical absorption spectra of the samples. We deduced that although the magnitude of the optical absorption increased with increasing implantation fluence, the shape of the absorption curve was the same for all samples.

Absorption spectra contain useful information about the size and shape of a system of metal nanoparticles.[3] A sample

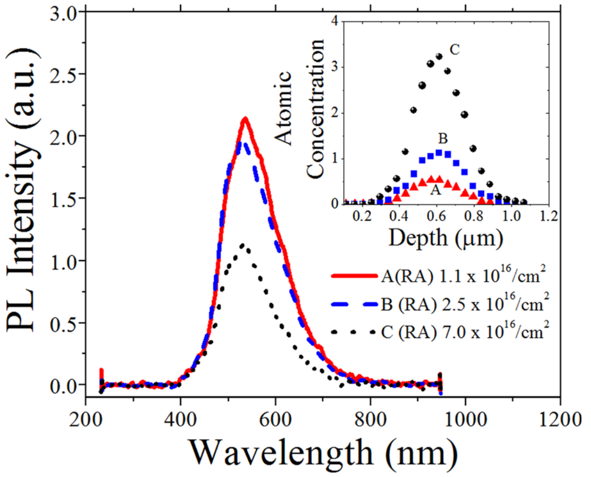

FIG. 3. Photoluminescence spectra of Pt nanoclusters embedded in a silica matrix obtained by implanting the Pt ions at fluencies of: (A) $1.1 \times 10^{16}\,\mathrm{cm}^{-2}$, (B) $2.5 \times 10^{16}\,\mathrm{cm}^{-2}$, and (C) $7.0 \times 10^{16}\,\mathrm{cm}^{-2}$, and thermally annealed under a reducing atmosphere at 600 °C. The inset shows the depth profile of each sample measured by RBS. Excitation was at 355 nm.

containing nanoparticles of the same sizes and shape would exhibit a similar optical absorption curve. The intensity of the optical absorption is related to the size and number of nanoclusters present in the sample. The increased light absorption of a larger number of nanoclusters may also contribute to an increase in the PL intensity. The inset of Figure 4 shows the PL intensity vs fluence under irradiation at 355 nm for the samples with the highest (C) and lowest (A) implantation fluencies. At all pump laser fluencies, the PL intensity of sample A was higher than that of sample C. This result can be understood using a simple two-level model for PL excitation.[47–49] Assuming that the duration of the laser pulses (26 ps) is shorter than the PL lifetime, the number of Pt-ncs emitters (N^*) in the excited state at the end of the laser pulse is given by[47–49]

$$N^* = N(1 - e^{\sigma_{exc}\varphi\Delta t}), \tag{1}$$

where N is the maximum number of excitable and independent Pt-ncs emitters, φ is the photon flux, Δt is the duration of the laser pulse, and σ_{exc} is the effective excitation cross-section. The number of photons per cm^2 per pulse $\varphi\Delta t$ can be replaced by the pump pulse fluence Φ. In the linear regime, at low fluencies $N^* = N\sigma_{exc}\Phi$. Therefore, the slope of the curve in the inset of Figure 4 is related to the excitation cross-section of the nanoclusters (σ_{exc}) and the total number Pt-ncs that can emit light (N).[47–49] Assuming that σ_{exc} of each nanocluster is the same for both samples (A(RA) and C(RA)), which is reasonable considering their similar shape and size distributions, as we deduce from their absorption spectra, the number N of Pt-ncs that are able to emit light is higher for the sample that was generated at a lower implantation fluence. Although Sample C can absorb more light from the incoming beam, it has a lower PL emission intensity. Despite the greater number of Pt-ncs, the sample behaves as if it has a lower number of emitting Pt-ncs. This effect is known as concentration quenching luminescence,[50,51] caused by efficient energy transfer among the emitters. Above a certain emitter concentration, a decrease in PL occurs as the average distance between emitters becomes short enough to favor energy transfer.[50,51] Excitation is transferred among nearest neighbors and after a number of transfers, the excited state relaxes and the emitted photon can reach the detector. Consequently, the effective number of emitter Pt-ncs is reduced.

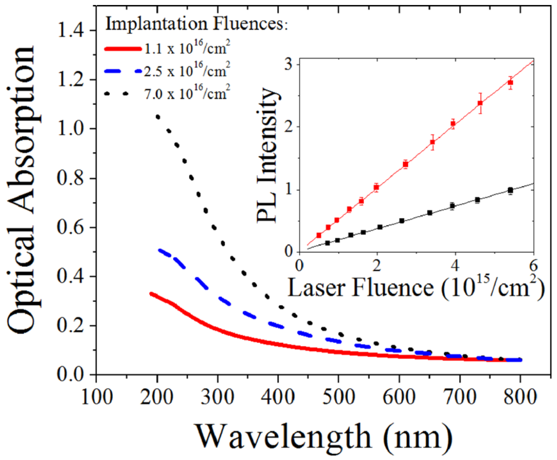

FIG. 4. Absorption spectra of silica samples with Pt nanoclusters obtained at three different Pt ions fluencies. The inset shows the photoluminescence intensity vs laser fluence of the samples with the highest ($7.0 \times 10^{16}\,\mathrm{cm}^{-2}$) and lowest fluencies ($1.1 \times 10^{16}\,\mathrm{cm}^{-2}$).

The average distance between the Pt-ncs plays a significant role in the energy-transfer process. From our RBS measurements (inset of Figure 3), we estimated the distance (d_{nc-nc}) between the Pt-ncs. Assuming average concentrations (from RBS) of 0.24×10^{21}, 0.43×10^{21}, and 1.3×10^{21} Pt cm^{-2} for samples A, B, and C, respectively, and considering the average diameter of the nanoclusters (1 nm from Figure 2), we estimated an average cluster numerical density ρ_{nc} of about 7.9×10^{-3}, 18×10^{-3}, and 50.5×10^{-3} Pt-ncs nm^{-3} for samples A, B, and C, respectively. These densities correspond to mean intercluster distances of 5.3, 4.3, and 2.9 nm for samples A, B, and C, respectively. Therefore, for the sample C(RA), the Pt-ncs are, on average, closer to each other. Energy transfer between emitters typically occurs at a separation of about 10 nm, and according to some theoretical models the efficiency of energy transfer processes scales as $1/d^4$, i.e., the process is more efficient with shorter separation between emitters.[50–53]

Pt-ncs embedded in silica show good potential for many technological applications in photonics and optoelectronics. For example, using a metal nanocluster as a nano-antenna may allow the electromagnetic emission from a Pt nanocluster to be transferred to another PL emitting species, such as a Si nanocrystal. Si-NCs have been extensively studied and many approaches have been explored to enhance their PL efficiency.[54–60] In this work, we co-implanted Si and Pt in the same silica matrix to enhance the PL emission from Si-NCs and form luminescent Pt-ncs. The depth concentration profile of this hybrid system is shown in Figure 5. First, we implanted Si ions to form Si-NCs, whose PL spectrum is shown in Figure 6. Pt ions were then implanted to avoid spatial overlap with the Si ion distribution (see Figure 5).

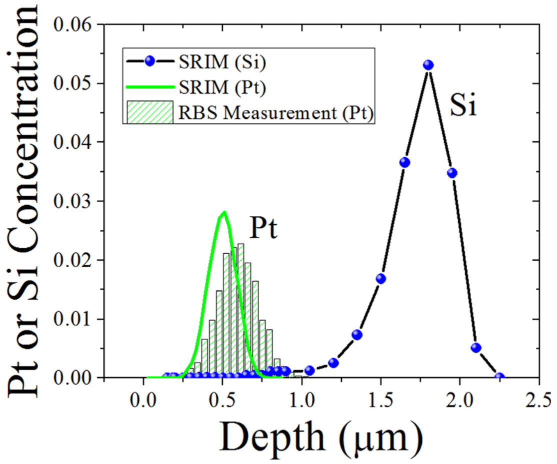

FIG. 5. Theoretical Si depth profile was determined with the SRIM program. Si ions were implanted at 1.5 MeV. The Pt depth profile was measured by RBS. Pt ions were implanted at 1.9 MeV and an implantation fluence of $4.9 \times 10^{16}\,\mathrm{cm}^{-2}$.

The PL spectra of the Si and Pt implanted samples showed weak signals from the Si-NCs and Pt-ncs formed in the matrix. It is possible that some Pt ions reached the region where the Si-NCs nucleated. This may have damaged the Si-NCs and reduced the PL intensity of the system. The PL intensity from the Si-NCs was reduced by almost a factor of two, suggesting considerable damage from the Pt implantation. PL emission from the Si-NCs is size dependent and smaller Si-NCs are expected to emit light at shorter wavelengths because of quantum confinement effects.[56] Ion implanted Si-NCs in silica form nanocrystals with sizes in the range of 3–6 nm,[54,56] which explains the wide PL spectra (600–850 nm) of the samples with Si-NCs as shown in Figure 6. After Pt implantation, the PL spectra of the Si-NCs showed a lower intensity; however, the peak PL emission was unchanged. This indicated that the Pt ions damaged both small and large Si-NCs without affecting the overall Si-NC size distribution. Finally, the sample was thermally annealed at 600 °C under a RA. The thermal treatment enhances hydrogen diffusion inside the silica matrix to allow better hydrogen passivation of surface defects on the Si-NCs, enhancing their luminescent efficiency. The annealing step also induces nucleation of luminescent Pt-ncs.[54,55] The PL spectrum of this sample is shown in Figure 6. The PL intensity of the Si-NCs in the sample was clearly enhanced. Moreover, the PL from Pt-ncs formed inside the silica was also visible. Thermal annealing under a RA at 600 °C passivated the silica defects, so that the PL peak at 530 nm derived only from Pt-ncs formed inside the silica after ion implantation. The hybrid sample (Si-NCs+Pt-ncs) has also a higher optical density from the absorption of the two particle types, as shown in the inset of Figure 6. This luminescent hybrid system formed from metallic Pt and semiconductor Si nanoparticles featured a broad PL emission spectrum, which spanned the visible spectrum as shown in Figure 6. Thus, our hybrid system demonstrated bright white light emission.

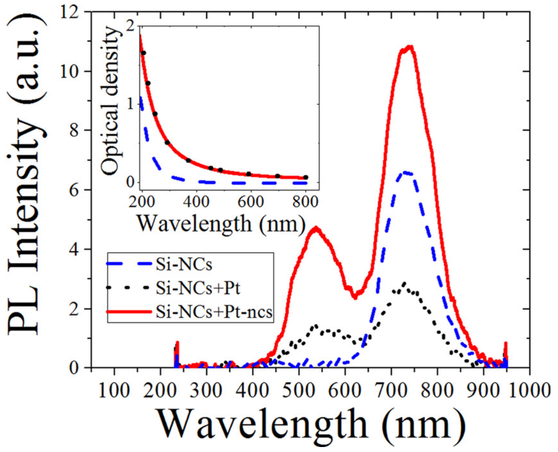

FIG. 6. Photoluminescence spectra of a silica sample with Si nanocrystals (blue dashed curve), Si nanocrystals and Pt ions (Si-NCs-Pt, black dotted curve), and Si nanocrystals and Pt nanoclusters (Si-NCs+Pt-ncs) embedded in silica matrices (red continuous curve). The excitation wavelength was 355 nm. The inset shows the optical absorption spectra of each sample.

The enhanced PL intensity from the Si-NCs is likely because of a combination of improved passivation of surface defect states on the Si-NCs and efficient energy transfer from the Pt-ncs to the Si-NCs. In the process of energy transfer, the Pt-ncs act as donors, which transfer their excitation to other species, including the Si-NCs.[50,51] This energy transfer mechanism enhances the absorption efficiency of the Si-NCs, leading to stronger PL emission. The intensity and PL decay time of the donor Pt-ncs decrease. This process is very efficient if some requirements are satisfied, including: (i) the donor Pt-ncs and acceptor Si-NCs are in close proximity to one another (typically 1 to 10 nm) and (ii) the luminescence spectrum of the donor Pt-ncs (400–600 nm) must overlap with the absorption or excitation spectra of the Si-NCs (UV–600 nm).[50,51] Another important characteristic of energy transfer processes is that the transfer rate (k_τ) is proportional to the photoluminescence decay rate τ_D^{-1} of the donor Pt-ncs. The PL decay times of Pt-ncs synthesized by chemical methods have been reported to be about 1–8 ns,[23–25] which is short enough to allow a rapid transfer rate between the Pt-ncs and Si-NCs, which typically have microsecond lifetimes.[55] The Si-NCs sample that was implanted with Pt but not annealed exhibited only weak PL emission from Pt-ncs and Si-NCs. The weak PL emission from the Pt-ncs may be explained taking into account the formation of Pt-ncs due to sample heating during the Pt-ion implantation. The thermal treatment at 600 °C allowed for a complete nucleation of the implanted Pt ions, and increased the number of Pt-ncs inside the silica, leading to a higher PL intensity. A larger number of Pt-ncs reduces the average separation between the Pt-ncs and Si-NCs in the region where the two ion distributions overlap.

Although we have obtained enhanced PL emission from Si-NCs in the presence of Pt-ncs, it is necessary to perform further studies, including time resolved photoluminescence to discriminate the contributions from two possible effects: improvements in passivation of Si-NCs defects and efficient energy transfer between Pt-ncs and Si-NCs. Our future work will focus on creating a hybrid system in which the optical interaction between these two kinds of emitters would be more efficient by making them closer to each other.

IV. CONCLUSIONS

We studied photoluminescence from ion implanted Pt nanoclusters in silica synthesized using a thermal treatment at 600 °C under three different atmospheres: air, argon, and a reducing atmosphere (H_2 and N_2). The photoluminescence spectra of Pt nanoclusters synthesized under these annealing conditions were similar, featuring a broad emission (400–600 nm) peaking at about 530 nm. We also studied a hybrid system made of Si nanocrystals and Pt nanoclusters embedded in silica. The observed photoluminescence spectrum of this hybrid sample covered the entire visible spectrum. Moreover, the photoluminescence intensity of the Si nanocrystals was enhanced after nucleation of the Pt nanoclusters, which we attributed to two effects: improved passivation of surface defects on the Si nanocrystals by hydrogen and efficient energy transfer between Pt nanoclusters and Si nanocrystals. Luminescent emitters made of Pt nanoclusters embedded in silica are an interesting light source with potential applications in photonics and optoelectronics.

ACKNOWLEDGMENTS

The author wishes to acknowledge Conacyt for its financial support through Grant No. 222485. Thanks to K. Lopez and F. J. Jaimes for running the accelerator, J. G. Morales for his assistance during sample preparation, and Matthew Tippett for technical help with the English version. We also wish to acknowledge the Laboratory for Nanoscience and Nanotechnology Research-LINAN of IPICYT for STEM characterization facilities.

[1] H. A. Atwater, Sci. Am. **296**, 56–62 (2007).
[2] W. L. Barnes, A. Dereux, and T. W. Ebbesen, Nature **424**, 824–830 (2003).
[3] K. L. Kelly, E. Coronado, L. L. Zhao, and G. C. Shatz, J. Phys. Chem. B **107**, 668–677 (2003).
[4] P. Anger, P. Bharadwaj, and L. Novotny, Phys. Rev. Lett. **96**, 113002 (2006).
[5] S. Kuhn, U. Hakanson, L. Rogobete, and V. Sandoghdar, Phys. Rev. Lett. **97**, 017402 (2006).
[6] H. Mertens and A. Polman, Appl. Phys. Lett. **89**, 211107 (2006).
[7] H. Xu and K. S. Suslick, Adv. Mater. **22**, 1078–1082 (2010).
[8] J. Zheng, C. Zhang, and R. M. Dickson, Phys. Rev. Lett. **93**, 077402 (2004).
[9] B. Santiago-González, M. J. Rodríguez, C. Blanco, J. Rivas, M. A. López-Quintela, and J. M. Gaspar-Martinho, Nano Lett. **10**, 4217–4221 (2010).
[10] J. Zheng, P. R. Nicovich, and R. M. Dickson, Annu. Rev. Phys. Chem. **58**, 409–431 (2007).
[11] T. P. Bigioni, R. L. Whetten, and Ö. Dag, J. Phys. Chem. B. **104**, 6983–6986 (2010).
[12] J. P. Wilcoxon, J. E. Martin, F. Parsapour, B. Wiedenman, and D. F. Kelley, J. Chem. Phys. **108**, 9137–9143 (1998).
[13] L. Khriachtchev, L. Heikkila, and T. Kuusela, Appl. Phys. Lett. **78**, 1994 (2001).
[14] G. Wang, T. Huang, R. W. Murray, L. Menard, and R. G. Nuzzo, J. Am. Chem. Soc. **127**, 812–813 (2005).
[15] S. Link, A. Beeby, S. FitzGerald, M. A. El-Sayed, T. G. Schaaff, and R. L. Whetten, J. Chem. Phys. B **106**, 3410–3415 (2002).
[16] J. Li, J.-J. Zhu, and K. Xu, Trends Anal. Chem. **58**, 90–98 (2014).
[17] M. Fukushima, N. Managaki, M. Fujii, H. Yanagi, and S. Hashayi, J. Appl. Phys. **98**, 024316 (2005).
[18] E. Trave, G. Mattei, P. Mazzoldi, G. Pellegrini, C. Scian, C. Maurizio, and G. Battaglin, Appl. Phys. Lett. **89**, 151121 (2006).
[19] C. Maurizio, E. Trave, G. Perotto, V. Bello, D. Pasqualini, P. Mazzoldi, G. Battaglin, T. Cesca, C. Scian, and G. Mattei, Phys. Rev. B **83**, 195430 (2011).
[20] H. Kawasaki, H. Yamamoto, H. Fujimori, R. Arakawa, M. Inada, and Y. Iwasaki, Chem. Commun. **46**, 3759–3761 (2010).
[21] P. N. Duchesne and P. Zhang, Nanoscale **4**, 4199–4205 (2012).
[22] X. Huang, K. Aoki, H. Ishitobi, and Y. Inouye, ChemPhysChem **15**, 642–646 (2014).
[23] S.-I. Tanaka, K. Aoki, A. Muratsugu, H. Ishitobi, T. Jin, and Y. Inouye, Opt. Mater. Express **3**, 157–165 (2013).
[24] X. L. Guevel, V. Trouillet, C. Spies, G. Jung, and M. Schneider, J. Phys. Chem. C **116**, 6047–6051 (2012).
[25] S.-I. Tanaka, J. Miyasaki, D. K. Tiwari, T. Jin, and Y. Inouye, Angew. Chem. Int. Ed. **50**, 431–435 (2011).
[26] C.-Y. Kang, C.-H. Chao, S.-C. Shiu, L.-J. Chou, M.-T. Chang, G.-R. Lin, and C.-F. Lin, J. Appl. Phys. **102**, 073508 (2007).
[27] R. Giulian, P. Kluth, L. L. Araujo, D. J. Llewellyn, and M. C. Ridgway, Appl. Phys. Lett. **91**, 093115 (2007).
[28] R. Giulian, P. Kluth, B. Johannessen, L. L. Araujo, D. J. Llewellyn, D. J. Cookson, and M. C. Ridgway, Nucl. Instrum. Methods Phys. Res. B **257**, 33–36 (2007).
[29] R. Giulian, L. L. Araujo, P. Kluth, D. J. Sprouster, C. S. Schnohr, B. Johannessen, G. J. Foran, and M. C. Ridgway, J. Appl. Phys. **105**, 044303 (2009).
[30] J. Bornacelli, H. G. Silva-Pereyra, L. Rodríguez-Fernández, M. Avalos-Borja, and A. Oliver, J. Lumin. **179**, 8–15 (2016).
[31] S. Manna, R. Aluguri, R. Bar, S. Das, N. Prtljaga, L. Pavesi, and S. K. Ray, Nanotechnology **26**, 045202 (2015).
[32] See http://www.srim.org/ for information about software packages and typical applications.
[33] J. F. Ziegler, M. D. Ziegler, and J. P. Biersack, Nucl. Instrum. Methods Phys. Res. B **268**, 1818–1823 (2010).
[34] J. A. Leavitt, L. C. McIntyre, Jr., and M. R. Weller, "Backscattering spectrometry," in *Handbook of Modern Ion Beam Materials Analysis*, edited by J. R. Tesmer and M. Nastasi (Mater. Res. Soc. Symp. Proc., 1995).
[35] A. Oliver, J. C. Cheang-Wong, A. Crespo *et al.*, Mater. Sci. Eng., B **78**, 32–38 (2000).
[36] M. Watanabe, S. Juodkazis, H. B. Sun, S. Matsuo, and H. Misawa, Phys. Rev. B **60**, 9959 (1999).
[37] L. Skuja, M. Hirano, H. Hosono, and K. Kajihara, Phys. Status Solidi C **2**, 15–24 (2005).
[38] L. Skuja, J. Non-Cryst. Solids **239**, 16–48 (1998).
[39] Y. Sakurai and K. Nagasawa, J. Appl. Phys. **88**, 168 (2000).
[40] H. Nishikawa, E. Watanabe, D. Ito, Y. Sakurai, K. Nagasawa, and Y. Ohki, J. Appl. Phys. **80**, 3513 (1996).
[41] Y. Sakurai and K. Nagasawa, J. Non-Cryst. Solids **277**, 82 (2000).
[42] P. W. Wang, R. F. Haglund, Jr., D. L. Kinser, M. H. Mendenhall, N. H. Tolk, and R. A. Weeks, J. Non-Cryst. Solids **102**, 288 (1988).
[43] Y. Sakurai and K. Nagasawa, J. Appl. Phys. **86**, 1377 (1999).
[44] I. Diez and R. H. A. Ras, Nanoscale **3**, 1963 (2011).
[45] B. Hammer and J. K. Norskov, Nature **376**, 238 (1995).
[46] C. Zhou, J. Wu, A. Nie, R. C. Forrey, A. Tachibana, and H. Cheng, J. Phys. Chem. C **111**, 12773–12778 (2007).
[47] M. Wojdak, M. Klik, M. Forcales, O. B. Gusev, T. Gregorkiewicz, D. Pacifici, G. Franzò, F. Priolo, and F. Iacona, Phys. Rev. B **69**, 233315 (2004).
[48] D. Kovalev, J. Diener, H. Heckler, G. Polisski, N. Künzner, and F. Koch, Phys. Rev. B **61**, 4485 (2000).
[49] D. Timmerman, I. Izeddin, and T. Gregorkiewicz, Phys. Status Solidi A **207**, 183–187 (2010).
[50] J. R. Lakowicks, *Principles of Fluorescence Spectroscopy*, 3rd ed. (Baltimore, Springer, 2006).
[51] J. García-Solé, L. E. Bausá, and D. Jaque, *An Introduction to the Optical Spectroscopy of Inorganic Solids* (England, John Wiley & Sons, Ltd., 2005).
[52] H. Kuhn, J. Chem. Phys. **53**, 101–108 (1970).
[53] T. Sen and A. Patra, J. Phys. Chem. C **112**, 3216–3222 (2008).
[54] J. Bornacelli, J. A. Reyes-Esqueda, L. Rodríguez-Fernández, J. L. Ruvalcaba-Sil, F. J. Jaimes, and A. Oliver, J. Nanotechnol. **2014**, 863184 (2014).

[55] J. Bornacelli, J. A. Reyes-Esqueda, L. Rodríguez-Fernández, and A. Oliver, J. Nanotechnol. **2013**, 736478 (2013).

[56] B. G. Fernandez, M. López, C. García, A. Pérez-Rodríguez, J. R. Morante, C. Bonafos, M. Carrada, and A. Clavarie, J. Appl. Phys. **91**, 798 (2002).

[57] A. R. Wilkinson and R. G. Elliman, J. Appl. Phys. **96**, 4018 (2004).

[58] M. Bolduc, G. Genard, M. Yedji, D. Barba, F. Martin, G. Tergawne, and G. G. Ross, J. Appl. Phys. **105**, 013108 (2009).

[59] A. R. Wilkinson and R. G. Elliman, Appl. Phys. Lett. **83**, 5512 (2003).

[60] J. S. Biteen, N. S. Lewis, H. A. Atwater, H. Mertens, and A. Polman, Appl. Phys. Lett. **88**, 131109 (2006).